IRS-Assisted DECT-2020 NR framework for Ensuring URLLC Constraints in Industrial IoT

Awais Bin Asif, Hassan Ahmad, and Jürgen Peissig
Institute of Communications Technology, Leibniz Universität Hannover, Germany
{asif,ahmad,peissig}@ikt.uni-hannover.de

***Abstract*—DECT 2020 NR is a Radio Interface Technology (RIT) introduced by ETSI for massive Machine Type Communications (mMTC) and Ultra-Reliable Low Latency Communications (URLLC) use cases. Notably, DECT 2020 NR stands as the sole non-cellular 5G technology apt for industrial IoT (IIoT) scenarios. However, achieving the stringent reliability and latency requirements of URLLC in dense industrial settings poses a significant challenge due to various propagation losses and severe shadowing. In this research work, we propose a novel DECT 2020 NR framework incorporating Intelligent Reflecting Surface (IRS) to meet the challenging URLLC constraints. The framework maps the system model in 3D space, including the 3D mapping of the radiation pattern of IRS, and employs the Separating Axis Theorem (SAT) to systematically identify shadowed regions within this 3D system model and mitigate the identified shadowed areas, leveraging the proposed novel MAC procedure for the IRS-assisted DECT 2020 NR network. Additionally, we propose a resource allocation scheme based on the priority given to radio devices ready to offload the data. Comparative analysis demonstrates that our proposed solution achieves significant improvements in received power, throughput, and reduction in round-trip time (RTT) when compared to both the existing approach and the conventional DECT 2020 NR standard.**

***Index Terms*—DECT 2020 NR, URLLC, IRS, Industrial IoT,**

I. Introduction

DECT 2020 NR, or DECT NR+, is a non-cellular Radio Interface Technology (RIT) for 5G private networks, released by ETSI in 2020. It supports mMTC and URLLC use cases under the IMT-2020 guidelines [1]. Operating in license-exempt and licensed sub-6GHz bands, DECT NR+ enables local, self-hosted deployments suited for industrial IoT (IIoT), factory automation, and energy grid monitoring [2]. It supports Radio Devices (RDs) operating in Fixed Termination (FT), Portable Termination (PT), and combined FT/PT modes, denoted as $\mathrm{RD}_{\mathrm{FT}}$, $\mathrm{RD}_{\mathrm{PT}}$, and $\mathrm{RD}_{\mathrm{FT/PT}}$, respectively.

In factory hall environments, obstacles like metallic racks and heavy machinery can severely attenuate signal strength. The standard DECT NR+ method [3] suggests a multi-cluster approach for reliability; however, it relies on flooding-based data transmission, which increases network resource usage and does not guarantee optimal end-to-end latency [4]. Additionally, radio devices in outage or obstructed by shadowing may experience long re-association delays with the gateway until signal conditions improve, posing challenges to meeting URLLC's strict reliability and latency demands.

Intelligent Reflecting Surfaces (IRS) have recently emerged as a promising technology to address signal blockage issues by leveraging reflection capabilities [5]. An IRS comprises an array of reflecting elements designed with periodic patterns that enable precise control over incident electromagnetic waves. This control facilitates functionalities such as directing the wave towards specific directions or fully absorbing it to prevent access by unauthorized users.

Current DECT NR+ literature primarily focuses on technology evaluation. In [6], [7], the authors assess DECT NR+ at the link and system levels for mMTC. A link-level evaluation for URLLC is presented in [8], confirming URLLC compliance. In [9], a MAC protocol is proposed to reduce outage probability and achieve 99.99% reliability in indoor industrial settings. It targets a single cluster and addresses packet routing via an intermediate node, using a broadcast mode-switch request from PT to FT/PT mode during outages. However, the node selection is suboptimal, and with the addition of each intermediate node nearly doubles the latency, increasing resource consumption [4].

Given the limitations of existing studies and the standard DECT NR+ approach, neither its default MAC protocol nor current research sufficiently meets URLLC requirements in dense industrial IoT environments. To address this, we propose a novel framework leveraging the DECT NR+ MAC layer [3] in conjunction with Intelligent Reflecting Surfaces (IRS) to achieve the required reliability and latency for URLLC. The framework constructs a 3D system model that includes the factory hall layout, initial positions of DECT NR+ radio devices, IRS pool dimensions, and physical obstacles like metallic racks. It applies the Separating Axis Theorem (SAT) on this 3D model to identify shadowed outage-prone regions. The IRS radiation pattern is then mapped in 3D space, considering directivity and half-power beamwidth toward those regions. Using this joint 3D mapping, the gateway assigns IRS elements to radio devices experiencing outages via a novel IRS-assisted DECT NR+ MAC procedure. Finally, after network initialization, the gateway allocates sub-slot resources based on a priority scheme favoring radio devices ready to offload data. Evaluation of the proposed approach against the DECT NR+ transmission configuration and existing methodologies [9] reveal enhancements in received power, throughput, and reductions in round-trip time. The remainder of this paper is organized as follows: Section II presents the system model, Section III outlines the proposed solution, Section IV evaluates performance using simulations, and Section V offers concluding remarks.

979-8-3503-9281-4/25/$31.00 ©2025 IEEE

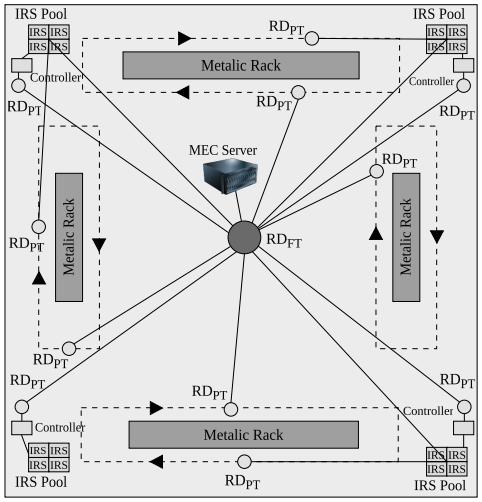

Fig. 1: System model

II. System Model

In this study, we investigate a DECT NR+ wireless network designed for an industrial IoT scenario with IRS integration, as illustrated in Fig. 1. The network includes a central gateway, denoted as $\mathrm{RD_{FT}}$, a set of DECT NR+ radio devices in PT mode, denoted as set $RD = \{RD_{PT_1}, RD_{PT_2}, ..., RD_{PT_n}\}$, and multiple IRS pools, denoted as $Ip = \{irsp_1 : \{irs_1, irs_2, ..., irs_k\}, irsp_2 : \{irs_1, irs_2, ..., irs_k\}, ..., irsp_n : \{irs_1, irs_2, ..., irs_k\}\}$. Each IRS pool is connected to an IRS controller, and each IRS controller is linked to an $\mathrm{RD_{PT}}$ to receive configuration instructions from the gateway. A mobile edge computing (MEC) server is also connected to the gateway. Positioned centrally in the factory hall, the $\mathrm{RD_{FT}}$ is supported by a set of IRSs to cover shadowed regions. The $\mathrm{RD_{PT}}$ devices, equipped with sensors and functioning as an automated guided vehicles (AGVs), follow a predefined mobility path to collect data, which is subsequently offloaded to the MEC server for processing.

Let $H_{g,i}$ denotes the channel gain from the gateway to irs_i, $G_{i,r}$ denotes the channel gain between irs_i and RD_{PT_r}, Φ_i denotes the phase shift of the irs_i. The IRS-assisted channel gain between the gateway and RD_{PT_r} is expressed as:

$$h^i_{g,r} = G_{i,r}\Phi_i H_{g,i} \tag{1}$$

The path loss model between the gateway and RD_{PT_r} is chosen from the IMT-2020 guidelines [1] which is expressed as:

$$PL_{g,r} = 16.9\log_{10}(d_{g,r}) + 32.8 + 20\log_{10}(f_c) \tag{2}$$

where $d_{g,r}$ is the distance from the gateway to RD_{PT_r}, and f_c is the operating frequency. The received power of the IRS-assisted channel from the gateway to RD_{PT_r} is expressed as:

$$P_{g,r} = \frac{G^g_t G^r_r G^i_t P_t}{PL^i_{g,r}} \tag{3}$$

where G^g_t is the transmitter gain of the gateway, G^r_r is the receiver gain of the RD_{PT_r}, G^i_t is the transmitter gain of the IRS, P_t is the transmit power of the gateway, and $PL^i_{g,r}$ is the pathloss of the IRS-assisted channel from the gateway to the RD_{PT_r}. The transmitter gain of the IRS is a function of the directivity, which is expressed as:

$$G^i_t = \varepsilon D \tag{4}$$

where ε is the efficiency of the IRS and D is the directivity of the IRS. According to the guidelines in [10], the efficiency of the IRS is chosen $\varepsilon = 0.9$. The directivity of the IRS is defined as the ratio of the radiation intensity of the reflected wave in a given direction to the radiation intensity averaged over all directions. The directivity of IRS is calculated using the method proposed in [10]. The expression of the directivity is given by:

$$D(\theta, \varphi) = \frac{4\pi U(\theta, \varphi)}{\int_0^{2\pi}\int_0^{\pi} U(\theta, \varphi)\sin\theta d\theta d\varphi} \tag{5}$$

where $U(\theta, \varphi)$ is the radiation intensity of IRS in the direction defined by θ and φ. To calculate the SNR, denoted as γ_r, at the RD_{PT_r}, the following expression is used:

$$\gamma_{g,r} = \frac{P_{g,r}}{N} \geq \gamma_t \tag{6}$$

where N is the noise power and γ_t is the SNR threshold value which is calculated using our previous work [8]. The SNR threshold value corresponds to the packet error rate to achieve the reliability requirement of URLLC. The maximum achievable data rate at the RD_{PT_r} is calculated using the formula given in equation (7).

$$R_{g,r}(n, \epsilon) = B\log_2(1 + \gamma_{g,r}) - \sqrt{\frac{V}{n}}Q^{-1}(\epsilon) \tag{7}$$

where B is the DECT NR+ supported bandwidth, V is the channel dispersion, n is the blocklength, ϵ is the error probability, and $Q^{-1}(\epsilon)$ is the inverse Q-function of the error probability. Based on the maximum achievable data rate and the data rate requirement of the application, a suitable Modulation and Coding Scheme (MCS) [2] is selected. DECT NR+ [2] supports various transmission configurations (μ, β) as shown in Table I.

The number of sub-slots required to transmit a packet is calculated by the following expression:

$$N_{\text{sub}} = \left\lceil \frac{\frac{S\cdot 8}{R_{g,r}}}{T^g_{\text{sub}}} \right\rceil \tag{8}$$

where S is the size of the packet in bytes, $R_{g,r}$ is the throughput of the link between gateway and RD_{PT_r} with unit bits per second (bps) calculated by the selected MCS, and T^g_{sub} is the subslot length in seconds given by the supported transmission configuration (μ, β) of the DECT NR+ standard [2]. Thus, the data packet transmission duration is given by:

$$t_{\text{dur}} = N_{\text{sub}} \cdot T^g_{\text{sub}} \tag{9}$$

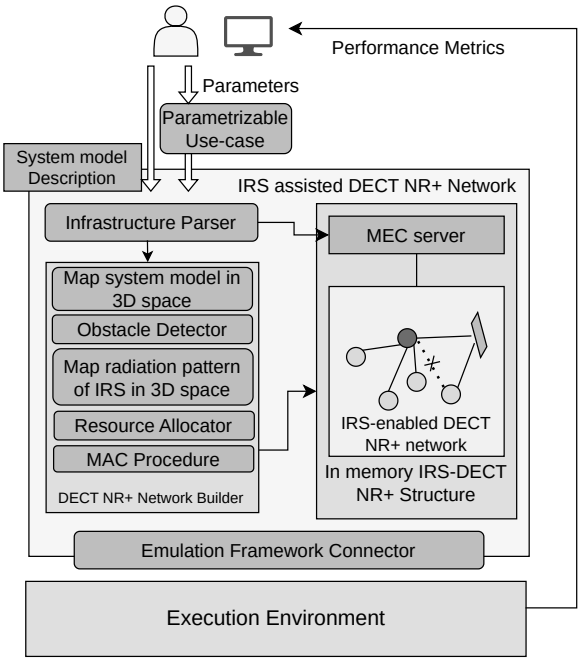

Fig. 2: System architecture

The total user-plane latency [11] for the DECT NR+ supported frame-based system operation without Hybrid Automatic Repeat request (HARQ) is expressed in equation (10).

$$T_{g,r}^{N} = t_{\text{sym}} + t_{\text{rd\_tx}} + t_{\text{FA\_switch}} + t_{\text{dur}} + t_{\text{rd\_rx}} \tag{10}$$

where t_{sym} is the symbol alignment time, $t_{\text{rd\_tx}}$ is the transmitter (TX) side processing delay, $t_{\text{FA\_switch}}$ is the TX alignment and TDD switching time, and $t_{\text{rd\_rx}}$ is the receiver (RX) side processing delay. The total user-plane latency with HARQ is calculated using the equation (11):

$$T_{g,r}^{H} = T_{g,r}^{N} + n \cdot [T_1 + T_2] \tag{11}$$

where n is the total number of re-transmissions. T_1 and T_2 are calculated by the following expressions.

$$T_1 = t_{\text{tx}} + t_{\text{FA\_switch}} + t_{\text{HARQ}} + t_{\text{rd-rx}} \tag{12}$$

$$T_2 = t_{\text{rd\_tx}} + t_{\text{FA\_switch}} + t_{\text{dur}} + t_{\text{rd\_rx}} \tag{13}$$

where T_1 represents HARQ feedback transmission delay and T_2 represents data re-transmission delay. In equation (12), t_{tx} is the TX side processing delay for HARQ feedback transmission, t_{HARQ} is the HARQ ACK/NACK transmission delay, $t_{\text{FA\_switch}}$ is the TX alignment and TDD switching time for HARQ ACK/NACK, and $t_{\text{rd-rx}}$ is the receiver side processing delay for ACK/NACK. The symbols in equation (13) are explained in equation (10). The detailed description of our proposed solution is presented in Section III.

III. Proposed Solution

We propose an innovative DECT NR+ framework designed to incorporate an IRS to uphold the reliability and latency requirements critical to URLLC-based IIoT networks. Fig. 2 provides a high-level overview of our proposed framework. The procedure begins with the network operator introducing high-level parameters into a parameterizable system model, outlining the configurations of an IRS-aided DECT NR+ wireless network. The system model description includes the properties of computing nodes, like Mobile Edge Computing (MEC) servers, the locations and properties of DECT NR+ radio devices (such as $\text{RD}_{\text{FT}_\text{s}}$, $\text{RD}_{\text{FT/PT}_\text{s}}$ and $\text{RD}_{\text{PT}_\text{s}}$), and the positions and parameters of IRS units (including IRS size, cell size, and the number of IRS states). Additionally, the model accounts for the characteristics of physical obstacles in the factory environment, such as the dimensions of the metallic racks, and all other necessary parameters to comprehensively describe a DECT NR+ network. Utilizing the system model description, the framework maps the radio devices, obstacles, and radiation pattern of the IRS in 3D space. Subsequently, the framework employs the Separating Axis Theorem (SAT) on 3D representations of both radio devices and obstacles to identify shadowed areas. Lastly, exploiting the 3D mapping of both the radio devices and the obstacles, alongside the identified shadowed zones and 3D mapping of IRS radiation patterns, the proposed MAC procedure is initiated for an IRS-aided DECT NR+ wireless network. Detailed explanations of each sub-module are provided in the subsequent sections.

A. Map system model in 3D space

Utilizing the system model, the framework begins by mapping the dimensions of the region of interest (ROI), specifically the factory hall. In 3D space, it is represented as $F = \{l_f, w_f, h_f\}$, where l_f, w_f, and h_f denote the length, width, and height, respectively. Radio devices are modeled as one cubic meter box and represented as $R = \{RD_1(rd_{id_1}, p_1, t_1), RD_2(rd_{id_2}, p_2, t_2), .., RD_n(rd_{id_n}, p_n, t_n)\}$, where rd_{id_n} is the ID, p_n the position, and t_n the type (FT, FT/PT, or PT) of the n^{th} radio device. $\text{RD}_{\text{PT}_\text{s}}$ are designated as AGVs, each following a predefined mobility path. These are represented as $A_g = \{agv_1(rd_{id_1}, m_1), agv_2(rd_{id_2}, m_2), ..., agv_n(rd_{id_n}, m_n)\}$, where m_n is the mobility path of the n^{th} RD_{PT}. IRS pools are mapped based on their location, size, unit cell dimensions, operating frequency, and orientation (horizontal/vertical). The IRS and unit cell sizes are given as $s \cdot \lambda$ and $\frac{\lambda}{d}$, where s and d are integers. Each pool contains k IRSs with $k \in [2, 4]$, represented as $I_p = \{irs_{p_1} : \{irs_1, irs_2, .., irs_k\}, irs_{p_2} : \{irs_1, irs_2, .., irs_k\}, ..., irs_{p_n} : \{irs_1, irs_2, .., irs_k\}\}$. Obstacles like metallic racks are modeled using the 3D coordinates of their vertices, forming polyhedra: $P = \{s_1(l_1), s_2(l_2), .., s_n(l_n)\}$, where s_n is the n^{th} side defined by coordinates l_n.

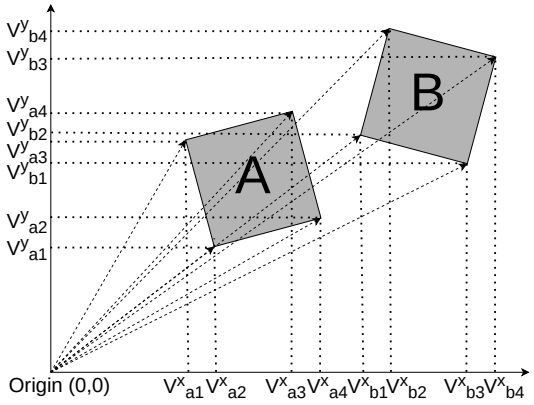

Fig. 3: Separating axis theorem in 2D space

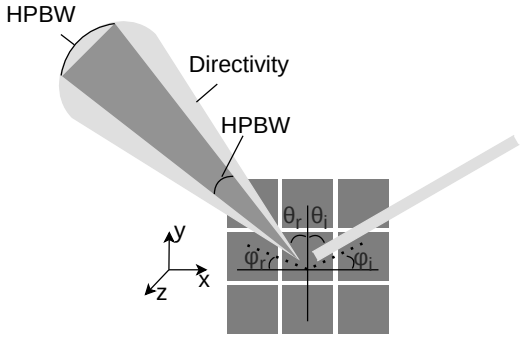

Fig. 4: 3D mapping of radiation pattern of IRS

B. Obstacle Detector

This sub-module utilizes the Separating Axis Theorem (SAT) to identify obstacles between the transmitter, specifically the gateway, and the $\mathrm{RD}_{\mathrm{PT_s}}$, in order to detect shadowed regions within the ROI. SAT is a computational geometry algorithm used to determine the collision or overlap between two convex polygons in 3D space. According to the SAT, two convex polygons do not overlap if and only if there exists a line along which their projections do not intersect. Fig. 3 demonstrates the application of the SAT algorithm to detect overlap between two squares, A and B, in a 2D space. The vectors representing the vertices of square A are v_{a_1}, v_{a_2}, v_{a_3}, and v_{a_4}, while those for square B are v_{b_1}, v_{b_2}, v_{b_3}, and v_{b_4}. Furthermore, the vector projections of squares A and B along the $x-axis$ and $y-axis$ are represented as $v^x_{a_1}$, $v^x_{a_2}$, $v^x_{a_3}$, $v^x_{a_4}$, $v^x_{b_1}$, $v^x_{b_2}$, $v^x_{b_3}$, $v^x_{b_4}$ and $v^y_{a_1}$, $v^y_{a_2}$, $v^y_{a_3}$, $v^y_{a_4}$, $v^y_{b_1}$, $v^y_{b_2}$, $v^y_{b_3}$, $v^y_{b_4}$, respectively. Squares A and B will overlap along the $x-axis$ if the following conditions are satisfied.

$$if(min(v^x_{b_1}, v^x_{b_2}, v^x_{b_3}, v^x_{b_4}) < max(v^x_{a_1}, v^x_{a_2}, v^x_{a_3}, v^x_{a_4})) \quad \{\text{Overlaps along x\_axis}\} \tag{14}$$

Similarly, squares A and B overlap along the $y-axis$ if following condition is satisfied:

$$if(min(v^y_{b_1}, v^y_{b_2}, v^y_{b_3}, v^y_{b_4}) < max(v^y_{a_1}, v^y_{a_2}, v^y_{a_3}, v^y_{a_4})) \quad \{\text{Overlaps along y\_axis}\} \tag{15}$$

To ascertain whether squares A and B overlap in a 2D space, both Equation (14) and Equation (15) must hold true. Extending this to 3D space, it is essential that the condition along the z-axis is also satisfied, in addition to the conditions in Equations (14) and (15). Furthermore, for polyhedrons to overlap in 3D space, they must exhibit overlap along the $x-axis$, $y-axis$, and $z-axis$, as well as along the vectors that are orthogonal to each face of the polyhedron.

To identify shadowed regions, a straight line is assumed between the transmitter (gateway) and receiver (AGV), representing a line of sight (LOS). The SAT is applied to the line and the 3D obstacle map, modelled as polyhedra. LOS is confirmed if Equations (14), (15), and the overlap conditions along vectors orthogonal to each obstacle face are satisfied. The AGV follows its mobility path with a 1-meter step size, using the obstacle detector to locate outage-prone shadowed areas. Nearby outage locations are clustered and represented as $O = \{o_1, o_2, ..., o_n\}$, where each o_i denotes a 3D coordinate of the identified outage location. After scanning the ROI, we obtain these outage sets and compute their centroids, forming the set $C = \{C_1, C_2, ..., C_n\}$, which is used in the next sub-module to map the IRS radiation pattern.

C. Map radiation pattern of IRS in 3D space

In this work, we consider metasurface-based IRS [10] and define the radiation pattern of the reflected wave using the directivity expression in equation (21). IRS directivity depends on the angle of incidence and angle of reflection of the incoming wave, as well as IRS properties such as its size, the size of reflecting elements, the number of states, and operating frequency.

Let Φ denote the IRS reflection phase, with $\Phi_x = \frac{\partial \Phi}{\partial x}$ and $\Phi_y = \frac{\partial \Phi}{\partial y}$ representing the desired phase gradients along the x and y axes, respectively. The phase of the mn-th IRS unit cell is given by:

$$\Phi_{mn} = (\frac{\partial \Phi}{\partial x} m + \frac{\partial \Phi}{\partial y} n) D_u + \Phi_{00} \tag{16}$$

where D_u denotes the unit cell size of the IRS, and Φ_{00} is the phase of its first unit cell. To relate the incidence angles of the impinging wave, θ_i and φ_i, to the reflection angles, θ_r and φ_r, the momentum conservation law for wave vectors is applied as follows:

$$\begin{aligned} \Phi_x &= k_r \sin\theta_r \cos\varphi_r - k_i \sin\theta_i \cos\varphi_i, \\ \Phi_y &= k_r \sin\theta_r \sin\varphi_r - k_i \sin\theta_i \sin\varphi_i, \end{aligned} \tag{17}$$

where $k_r = \frac{2\pi}{\lambda_r}$ and $k_i = \frac{2\pi}{\lambda_i}$ are the wave vectors of the reflected and incident mediums with wavelengths λ_r and λ_i, respectively. The target phase of the mn-th unit cell of IRS

for the normal incidence wave, i.e., $\theta_i = 0$ can be expressed as [10]:

$$\Phi_{mn} = \frac{2\pi D_u(m\cos\varphi_r \sin\theta_r + n\sin\varphi_r \sin\theta_r)}{\lambda_0} \quad (18)$$

where λ_0 is the wavelength of the normal incidence wave. Further, using the Huygens principle in the far-field limit, the scattering field can be expressed as [10]:

$$E(\theta,\varphi) = K\cos\theta \sum_{m=1}^{M}\sum_{n=1}^{N} \Gamma_{mn} e^{j[\Phi_{mn}+k_0\zeta_{mn}(\theta,\varphi)]} \quad (19)$$

where K is a constant defined by the amplitude of the incident wave, Γ_{mn} is the reflection coefficient, M and N are the numbers of unit cells along the IRS rows and columns, k_0 is the wave number, and $\zeta_{mn}(\theta,\varphi)$ denotes the relative phase shift of the unit cell at coordinates (θ,φ), given by:

$$\zeta_{mn}(\theta,\varphi) = D_u \sin\theta[(m-\frac{1}{2})\cos\varphi + (n-\frac{1}{2})\sin\varphi] \quad (20)$$

Lastly, the directivity of IRS is expressed as:

$$D(\theta,\varphi) = \frac{4\pi U(\theta,\varphi)}{\int_0^{2\pi}\int_0^{\pi} U(\theta,\varphi)\sin\theta d\theta d\varphi} \quad (21)$$

where $U(\theta,\varphi) \propto |E(\theta,\varphi)|^2$ denotes the radiation intensity scattered in a given direction. The Half Power Beam Width (HPBW) is calculated by taking the square root of the solid angle at the -3 dB point of a lobe's peak, as shown in Fig. 4. We use HPBW to map the IRS radiation pattern in 3D space. Let h_d be the HPBW in degrees; the corresponding arc length at a distance d is computed using equations (22) and (23).

$$h_r = h_d \cdot \frac{\pi}{180} \quad (22)$$

$$L = d \cdot h_r \quad (23)$$

where h_r denotes the HPBW in radians, L represents the arc length of the HPBW, and d is the distance from the IRS to the outage location. If $L > D_l$, where D_l is the size of the IRS, the radiation pattern is modelled as a trapezoidal prism. Conversely, if $L = D_l$, the radiation pattern is represented as a rectangular prism. Let $C_1 = (x_c, y_c, z_c) \in C$ denote the 3D coordinates of the outage location as identified by the Obstacle Detector, and let $B = (x_b, y_b, z_b)$ represent the 3D coordinates of the center of IRS. The mapping of the IRS radiation pattern to either a trapezoidal prism or a rectangular prism is determined as follows:

Step 1: Compute normalized directional vector:

$$\begin{aligned}\vec{v} &= \mathrm{B} - \mathrm{C}_1 = (x_b - x_c, y_b - y_c, z_b - z_c)\\ \hat{v} &= \frac{\vec{v}}{|\vec{v}|} = \frac{\vec{v}}{\sqrt{(x_b-x_c)^2 + (y_b-y_c)^2 + (z_b-z_c)^2}}\end{aligned} \quad (24)$$

Step 2: Find two unit vectors perpendicular to $\vec{v}$:
Select an arbitrary vector $(1,0,0)$ or $(0,1,0)$ or $(0,0,1)$ that is not parallel to $\vec{v}$ and calculate two unit vectors perpendicular to the vector $\vec{v}$. Let $\vec{a}$ be an arbitrary vector. Two perpendicular unit vectors, denoted as $\hat{u_1}$ and $\hat{u_2}$, are calculated as follows:

$$\begin{aligned}\hat{u_1} &= \frac{\vec{v}\times\vec{a}}{|\vec{a}\times\vec{v}|}\\ \hat{u_2} &= \frac{\vec{v}\times\hat{u_1}}{|\vec{v}\times\hat{u_1}|}\end{aligned} \quad (25)$$

Step 3: Find side of trapezoidal prism or rectangular prism parallel to IRS

$$\begin{aligned}h_1 &= C_1 + \frac{L}{2}\cdot\hat{u_1}\\ h_2 &= C_1 - \frac{L}{2}\cdot\hat{u_1}\\ v_1 &= C_1 + \frac{L}{2}\cdot\hat{u_2}\\ v_2 &= C_1 - \frac{L}{2}\cdot\hat{u_2}\end{aligned} \quad (26)$$

where 3D coordinates (h_1, h_2, v_1, v_2) define one side of a trapezoidal or rectangular prism oriented parallel to the IRS at position C_1. To determine the opposite side, the coordinates at C_1 are interchanged with those at point B, and the procedure outlined in Step 1, Step 2, and Step 3 is repeated. This results in a set of eight 3D coordinates, denoted as $R_1 = [(h_1, h_2, v_1, v_2), (h_3, h_4, v_3, v_4)]$ fully characterizing the trapezoidal or rectangular prism shape. The arrangement R_1 signifies the IRS radiation pattern oriented towards the location C_1. The framework leverages the calculated centroids of shadowed regions, as detailed in Section III-B, to effectively map the IRS radiation pattern towards each centroid, as expressed below:

$$\begin{aligned}&R_c = \{c_1 : \{r_1, r_2, .., r_n\}, c_2 : \{r_1, r_2, .., r_n\}\},\\ &c_3 : \{r_1, r_2, ..r_n\}, ..., c_n : \{r_1, r_2, ..r_n\}\},\\ &where\ \forall_i^n r_i \in irs_{p_i}\ and\ irs_{p_i} \neq irs_{p_j}\ \forall i \neq j\end{aligned} \quad (27)$$

where c_n represents the 3D coordinates of the n^{th} centroid, while $\{r_1, r_2, .., r_n\}$ denotes the set of radiation patterns directed from n IRS units towards the location c_n. The term irs_{p_i} refers to the i^{th} IRS pool, as defined in Section III-A. The constraints outlined in Equation (27) ensure the selection of a single IRS from the IRS pool for each centroid.

TABLE I: Transmission configuration

Properties	Config1	Config2	Config3	Config4
(μ, β)	(1,1)	(2,1)	(4,1)	(8,1)
Bandwidth (MHz)	1.728	3.456	6.912	13.824
Symbol Length (μs)	41.667	20.833	10.417	5.208
Subcarrier Spacing (kHz)	27	54	108	216
Subslot Length (ms)	0.208	0.104	0.052	0.0260

D. Resource Allocator

We propose a resource allocation scheme focused on subslot allocation by assigning a priority to RD_{PT_s} that are ready to offload the data. RD_{PT_s} advertise the amount of data to offload, exploiting the MAC layer functionalities of DECT NR+

specifically MAC Service Data Units (SDUs) multiplexed into a MAC Protocol Data Unit (PDU), as illustrated in Fig. 5.

Let $Z(t) = \{Z_1(t), Z_2(t), Z_3(t), \ldots, Z_n(t)\}$ represent the set of data that the $\mathrm{RD}_{\mathrm{PT_s}}$ have advertised as ready for offloading. let $RD = \{RD_{PT_1}, RD_{PT_2}, ..., RD_{PT_n}\}$ be the set of $\mathrm{RD}_{\mathrm{PT_s}}$ connected to the gateway. The set $P = \{p_1, p_2, p_3, .., p_n\}$ indicates the priority for each $\mathrm{RD}_{\mathrm{PT}}$, where $\forall_i^n p_i \in \{0, 1\}$. Here, $p_i = 0$ signifies that RD_{PT_i} has no data for offloading, whereas $p_i = 1$ denotes that RD_{PT_i} is prepared to offload data. The set P consequently divides RD into two subsets: $RD_p = \{RD_{PT_1}, RD_{PT_2}, ..., RD_{PT_l}\}$ and $RD_q = \{RD_{PT_1}, RD_{PT_2}, ..., RD_{PT_m}\}$, where RD_p contains the devices with $p = 1$, and RD_q comprises those with $p = 0$. The sub-slot allocation scheme for radio devices within the sets RD_p and RD_q is defined as follows:

$$N_{sub}^{p} = \frac{100 + m \cdot w}{l + m} \tag{28}$$

$$N_{sub}^{q} = \frac{100 + m \cdot w}{l + m} - w \tag{29}$$

where N_{sub}^{p} and N_{sub}^{q} represent the percentage of sub-slots allocated within a DECT NR+ frame to each radio device in sets RD_p and RD_q, respectively. Here, l denotes the number of nodes in RD_p, and m is the number of nodes in RD_q. Based on the priority set P, we define an integer w, which represents the difference in sub-slot allocation between radio devices in the RD_p and RD_q sets. Equations (28) and (29) facilitate the allocation of additional sub-slots to high-priority radio devices while granting fewer sub-slots to those with lower priority. The total number of sub-slots allocated to the i^{th} radio device within a DECT NR+ frame, denoted as N_{sub}^{i}, is defined as follows:

$$\forall_{i=1}^{n} N_{sub}^{i} = \begin{cases} N_T^f \cdot N_{sub}^{p}, & if\ i \in RD_p \\ N_T^f \cdot N_{sub}^{q}, & if\ i \in RD_q \end{cases} \tag{30}$$

where $n = l + m$ represents the total number of $\mathrm{RD}_{\mathrm{PT_s}}$. N_T^f denotes the total number of available sub-slots in a frame, which is determined by the transmission configuration (μ, β) of DECT NR+ [2], as outlined in Table I. The total number of frames required to offload the advertised data is calculated as follows:

$$\forall_{i=1}^{n} N_{\mathrm{s}}^{i} = \left\lceil \frac{\frac{Z_i(t) \cdot 8}{R_{i,g}}}{T_{\mathrm{sub}}^{i}} \right\rceil \tag{31}$$

$$\forall_{i=1}^{n} N_f^i = \left\lceil \frac{N_s^i}{N_{sub}^i} \right\rceil \tag{32}$$

where N_{s}^{i} represents the total number of sub-slots required to offload the data $Z_i(t)$ from the i^{th} radio device. $R_{i,g}$ denotes the data rate between the i^{th} radio device and the gateway. The sub-slot length, defined by the DECT NR+ transmission configuration, is indicated by T_{sub}^{i}. Finally, N_f^i is the total number of frames necessary for the i^{th} radio device to complete the data offloading process.

The gateway integrates resource allocation information within the MAC Information Element (IE) message [3] by configuring the appropriate fields such as start sub-slot, length fields, $\mathrm{RD}_{\mathrm{ID}}$, repeat, and validity fields, utilizing N_f^i and N_{s}^{i} as calculated from equations (32) and (31), respectively. The MAC IE message is then combined with a MAC multiplexing header and a unicast header of the convergence layer [12]. Each radio device (RD) connected to the gateway receives the Resource Allocation IE elements from the gateway, allowing them to reserve the necessary sub-slots for uplink transmission.

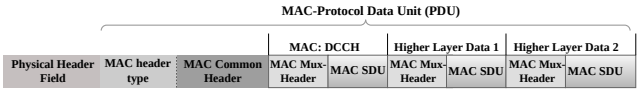

Fig. 5: Physical Header Field and Protocol Data Unit (PDU) of MAC layer.

E. MAC Procedure for IRS-assisted DECT NR+

After network initialization [3] and resource allocation, the DECT NR+ network supports uplink and downlink transmission. However, due to AGV mobility, the received power may drop below the required threshold, violating URLLC constraints. The gateway periodically evaluates AGV signal quality using the Measurement Report IE [3], which includes RSSI-2, SNR, and RSSI-1 values. If the received power falls below the threshold, the framework selects a suitable IRS to restore signal strength. Using the 3D IRS mapping from equation (27), the framework selects the set of IRS radiation pattern denoted as $R_p = \{r_1, r_2, ..., r_n\}$. The framework then applies SAT on $agv_p(rd_{id_p}, m_p)$ and each $r_n \in R_p$, selecting the radiation pattern that satisfies the condition defined in Section III-B. The SAT returns with the following three potential outcomes:

1) Case 1: SAT returns with one IRS

Let $r_i \in irs_{p_i}$ denote the radiation pattern selected by the SAT algorithm, where irs_{p_i} is the corresponding IRS pool. Each IRS pool is controlled by an IRS controller, paired with an $\mathrm{RD}_{\mathrm{PT}}$ to receive configuration commands from the gateway. The gateway generates the IRS configuration using an API such as [13] and embeds it into the MAC SDU and PDU with a unicast MAC header, including the $\mathrm{RD}_{\mathrm{ID}}$ of the $\mathrm{RD}_{\mathrm{PT}}$ connected to the IRS controller [3]. Upon receiving the message, the $\mathrm{RD}_{\mathrm{PT}}$ forwards the configuration to the IRS controller. The gateway then updates the IRS pool by removing r_i from the available IRS pool. For both uplink and downlink, we propose to reuse the previously allocated resources to $agv_p(rd_{id_p}, m_p)$, as outlined in Section III-D.

2) Case 2: SAT returns with no IRS

If the SAT algorithm finds no suitable IRS, it implies that the outage location is either beyond IRS coverage or the gateway's transmission power is insufficient for even single-hop communication. In such cases, we propose a multi-hop communication scheme to maintain the required reliability. The framework identifies the nearest possible intermediate radio device and sends a mode-switch request, prompting a

change from PT to FT/PT mode. This request is sent via a Cluster Beacon Message IE with a unicast header, setting the $\mathrm{RD}_{\mathrm{ID}}$ of the nearest radio device as the destination address. The agv_p (in outage) then associates with the selected intermediate AGV and performs uplink/downlink transmission to the gateway through this temporary node. Once agv_p moves into a region where either the gateway's beacon exceeds the threshold or IRS-assisted communication becomes feasible, it re-establishes direct connectivity with the gateway.

3) Case 3: SAT returns with more than one IRS

To determine the most appropriate IRS to utilize, the gateway assesses the AGV's trajectory and selects the IRS that the AGV is approaching. Let $\vec{p}(t) = (x_1, y_1, z_1)$ represent the 3D position vector of the AGV at time t, and $\vec{q}(t) = (x_2, y_2, z_2)$ denote the 3D position vector of IRS. The velocity vector of the AGV, $\vec{v}_p(t)$, indicates its movement direction at time t. This velocity vector characterizes the rate of change of displacement over time. It is mathematically expressed as follows:

$$\vec{v}_p(t) = \frac{d\vec{p}}{dt} = \left\langle \frac{dx_1}{dt}, \frac{dy_1}{dt}, \frac{dz_1}{dt} \right\rangle \tag{33}$$

The displacement vector from $\vec{p}(t)$ to $\vec{q}(t)$ is defined as follows:

$$\vec{d}(t) = \vec{q}(t) - \vec{p}(t) = \langle x_2(t) - x_1(t), y_2(t) - y_1(t), z_2(t) - z_1(t) \rangle \tag{34}$$

The gateway selects the considered IRS if the dot product $\vec{v}_p(t) \cdot \vec{d}(t) > 0$. The gateway then initiates the MAC procedure for IRS-assisted DECT NR+ downlink and uplink transmissions for the chosen IRS, as delineated in Case 1.

IV. Performance Evaluation

The performance of the proposed solution is evaluated using a topology consisting of one $\mathrm{RD}_{\mathrm{FT}}$ (gateway), eight $\mathrm{RD}_{\mathrm{PT_S}}$ devices deployed as AGVs, and four IRS pools, each containing four IRS units. Additionally, four static $\mathrm{RD}_{\mathrm{PT}}$ devices are connected to IRS controllers to receive configuration updates from the gateway, and a MEC server is connected to the gateway. The setup is within a factory hall of size 100×200×50 meters, with the gateway deployed at its center. The $\mathrm{RD}_{\mathrm{PT}}$ devices move along predefined paths at speeds up to 1 m/s, navigating around an obstacle, as shown in Fig. 1. We evaluate the proposed solution against four DECT NR+ transmission configurations (μ, β) listed in Table I. Simulation parameters include a 1.88 GHz operating frequency, IRS size of 5λ, unit cell size of $\frac{\lambda}{2}$, four IRS states, 32-byte packet size, and -88 dBm receiver sensitivity. The simulation of the proposed solution was implemented in Python. A detailed comparison is provided with an existing method [9] and the DECT NR+ standard [3]. In each run, mobile devices complete 1000 rounds at 1 m/s, sending one packet every meter. Received power is averaged over 1000 samples per step.

In the first experiment, we evaluate the proposed solution's performance against varying transmit power levels, as shown in Fig. 6. The results demonstrate that our approach consistently outperforms both the existing method [9] and the DECT NR+ standard [3]. By utilizing a 3D IRS radiation pattern map and a MAC procedure for IRS-assisted DECT NR+, our solution effectively detects shadowed areas and minimizes outage probability while meeting URLLC constraints. Fig. 6 shows that a minimum transmit power of 0 dBm is needed to maintain received power above the -88 dBm sensitivity threshold. In contrast, the existing approach [9] initiates mode switching request (PT to FT/PT) for all connected $\mathrm{RD}_{\mathrm{PT_s}}$ to route packets via intermediate nodes. However, the intermediate node selection is random, which fails to ensure optimal reliability, and multi-hop communication induces additional latency, conflicting with URLLC constraints. The DECT NR+ baseline performs the worst, as it relies on connecting to new FT or FT/PT nodes during outage, which is ineffective if all nearby nodes are in PT mode, leaving the affected device disconnected until signal conditions improve.

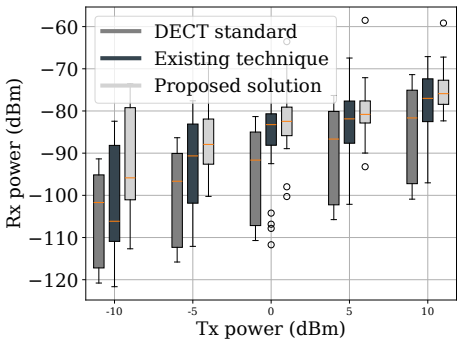

Fig. 6: Received power versus Transmit power

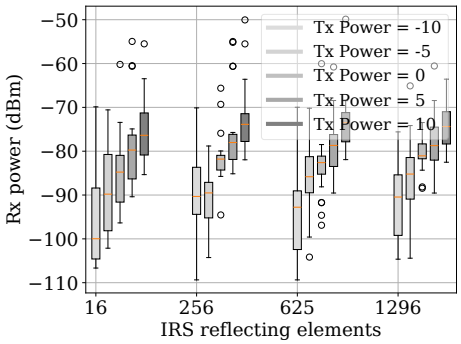

Fig. 7: Received power versus IRS reflecting elements

Fig. 7 evaluates the proposed solution with respect to the number of IRS reflecting elements and the transmit power of radio devices. Results show that at least 256 reflecting elements with 0 dBm transmit power are needed to meet the received power threshold. The IRS reaches saturation at 625 elements, as indicated in [5], with further increase in reflecting elements adding fabrication complexity. Fig. 8 presents the round-trip time (RTT) for data offloading between $\mathrm{RD}_{\mathrm{PTs}}$ and the gateway, which is connected to a MEC server. RTT is defined as the total duration for a packet to reach the gateway and return to the $\mathrm{RD}_{\mathrm{PT}}$. Link-level latency is computed via equation (11). Our solution outperforms both existing

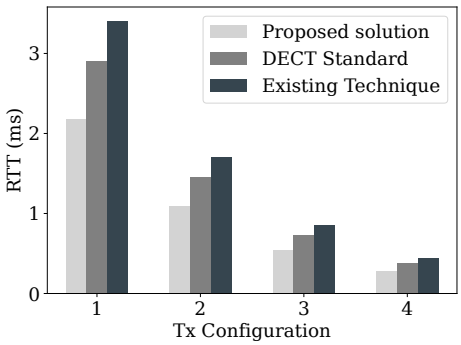

Fig. 8: RTT versus Tx configuration

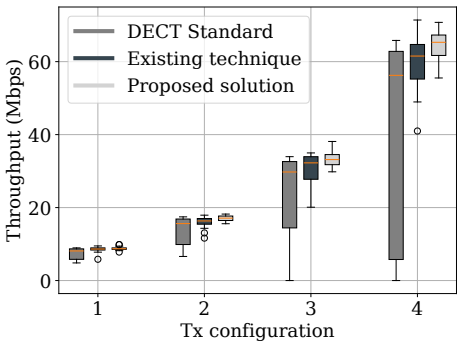

Fig. 9: Throughput versus Tx configuration

technique [9] and DECT NR+ standard approach, achieving high reliability by redirecting radio waves via IRS-assisted links, avoiding intermediate nodes and retransmissions. In contrast, [9] uses intermediate nodes to meet reliability targets, increasing latency. DECT NR+ relies on HARQ for reliable delivery, adding retransmission delays to RTT as defined in equations (12) and (13). Finally, throughput is analyzed for our method, [9], and DECT NR+ across four transmission configurations (μ, β) listed in Table I. Throughput is calculated as:

$$\eta = \frac{m \cdot S_p \cdot 8}{(T_{\text{end}} - T_{\text{start}}) \cdot 10^6} \tag{35}$$

where m is the number of successfully received packets, S_p is the packet size in bytes, T_{start} is the time when the first packet is sent by the gateway, and T_{end} is when the last packet is received at the destination. The proposed solution ensures reliable transmission without requiring retransmissions or intermediate nodes, minimizing transmission time and thereby achieving higher throughput compared to the existing technique [9] and the DECT NR+ default approach [3], as shown in Fig. 9. Throughput in DECT NR+ drops to zero for transmission configurations three and four due to severe shadowing and the higher sensitivity of wide bandwidths to noise. The proposed solution yields up to 10% improvement over both [9] and [3]. Moreover, the 3D mapping of the system and IRS radiation patterns is computed only once, introducing negligible additional time complexity for the proposed MAC procedure.

V. Conclusion

In this paper, we propose an innovative framework for IRS-assisted DECT NR+ within an Industrial Internet of Things (IIoT) context. The framework employs a 3D description of the system model to address shadowing issues encountered in such environments. Leveraging the Separating Axis Theorem (SAT) along with the 3D system model, our approach accurately identifies areas affected by shadowing. To address these shadowed regions, we propose a MAC procedure tailored for DECT NR+ that effectively mitigates the impact of shadowing. The evaluations demonstrate significant enhancements in received signal power, throughput, and a reduction in round-trip. For future work, we plan to incorporate deep learning techniques to further explore and refine the 3D mapping of system models in complex indoor industrial environments.

Acknowledgment

The work in this paper was part of the Celtic-Next project USWA and received funding from the Federal Ministry of Education and Research of Germany (BMBF, funding code: 16KISK254). We would like to thank the funding organization for the financial support.

References

[1] ITU-R, "Detailed specifications of the terrestrial radio interfaces of Inter-national Mobile Telecommunications-2020 (IMT-2020)," *International Telecommunication Union, Report ITU-R*, vol. M., pp. 2150–0, February 2021.

[2] ETSI, "DECT-2020 New Radio (NR); Part 3: Overview; Release 1," *European Telecommunications Standards Institute, Technical Specification (TS)*, vol. 103, pp. 636–3, March, 2024.

[3] ——, "DECT-2020 New Radio (NR); Part 4: MAC layer; Release 1," *European Telecommunications Standards Institute, Technical Specification (TS)*, vol. 103, pp. 636–4, March, 2024.

[4] A. B. Asif, H. Ahmad, S. Preihs, and J. Peissig, "Urllc-based multi-hop communication using dect-2020 nr," in *2025 IEEE Wireless Communications and Networking Conference (WCNC)*, 2025, pp. 1–7.

[5] A. B. Asif, C. Liaskos, A. Pitsillides, H. K. Qureshi, and M. Lestas, "Optimal Path Selection in Cascaded Intelligent Reflecting Surfaces," in *2022 IEEE 96th Vehicular Technology Conference (VTC2022-Fall)*, 2022, pp. 1–5.

[6] O. B. Smida, S. B. Amor, and S. Affes, "ETSI/DECT-2020 Component RIT Technology Implementation and Evaluation Contributions in mMTC and URLLC Use Cases," in *ICC 2023 - IEEE International Conference on Communications*, 2023, pp. 1462–1467.

[7] R. Kovalchukov, D. Moltchanov, J. Pirskanen, J. Säe, J. Numminen, Y. Koucheryavy, and M. Valkama, "DECT-2020 New Radio: The Next Step toward 5G Massive Machine-Type Communications," *IEEE Communications Magazine*, vol. 60, no. 6, pp. 58–64, 2022.

[8] M. Penner, M. Nabeel, and J. Peissig, "URLLC Performance Evaluation of IMT-2020 Candidate Technology: DECT-2020 New Radio," in *2021 IEEE 94th Vehicular Technology Conference (VTC2021-Fall)*, 2021, pp. 1–7.

[9] H. Ahmad, A. B. Asif, J. Peissig, and M. Penner, "Mac protocol for reducing outage probability in dect-2020 new radio," in *2024 20th International Conference on Wireless and Mobile Computing, Networking and Communications (WiMob)*, 2024, pp. 42–49.

[10] H. Taghvaee, S. Abadal, A. Pitilakis, O. Tsilipakos, A. C. Tasolamprou, C. Liaskos, M. Kafesaki, N. V. Kantartzis, A. Cabellos-Aparicio, and E. Alarcón, "Scalability Analysis of Programmable Metasurfaces for Beam Steering," *IEEE Access*, vol. 8, pp. 105 320–105 334, 2020.

[11] ETSI, "ETSI Evaluation Group; Final Evaluation Report on DECT-2020 NR," *European Telecommunications Standards Institute, Technical Report (TR)*, vol. 103, p. 810, Nov, 2021.

[12] ——, "DECT-2020 New Radio (NR); Part 5: DLC and Convergence layers; Release 1," *European Telecommunications Standards Institute, Technical Specification (TS)*, vol. 103, pp. 636–5, March, 2024.

[13] [Online]. Available: https://tmytek.com/products/components/xrifle-dynamic-ris